Electronic Supplementary Information

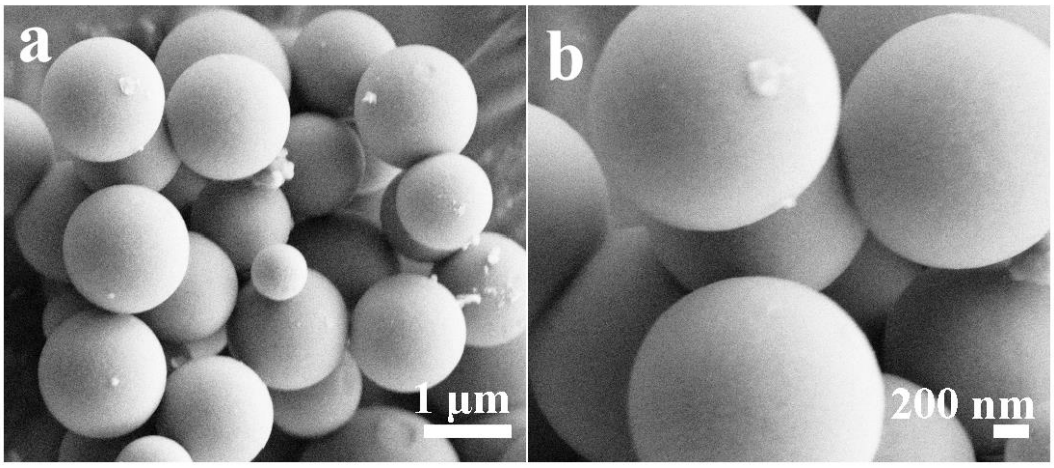

Fig. S1 (a, b) SEM images of NiZn-MOFs.

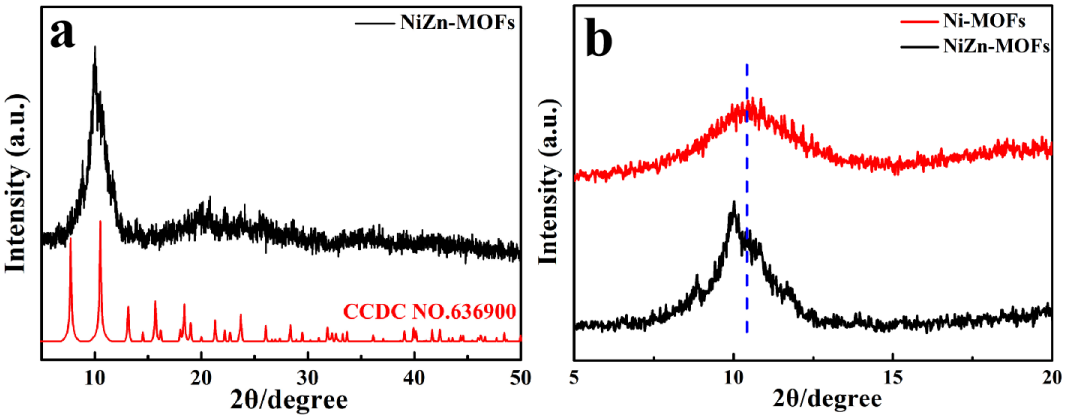

Fig. S2 (a) XRD pattern of NiZn-MOFs, (b) XRD patterns of NiZn-MOFs and Ni-MOFs from 5° to 20°.

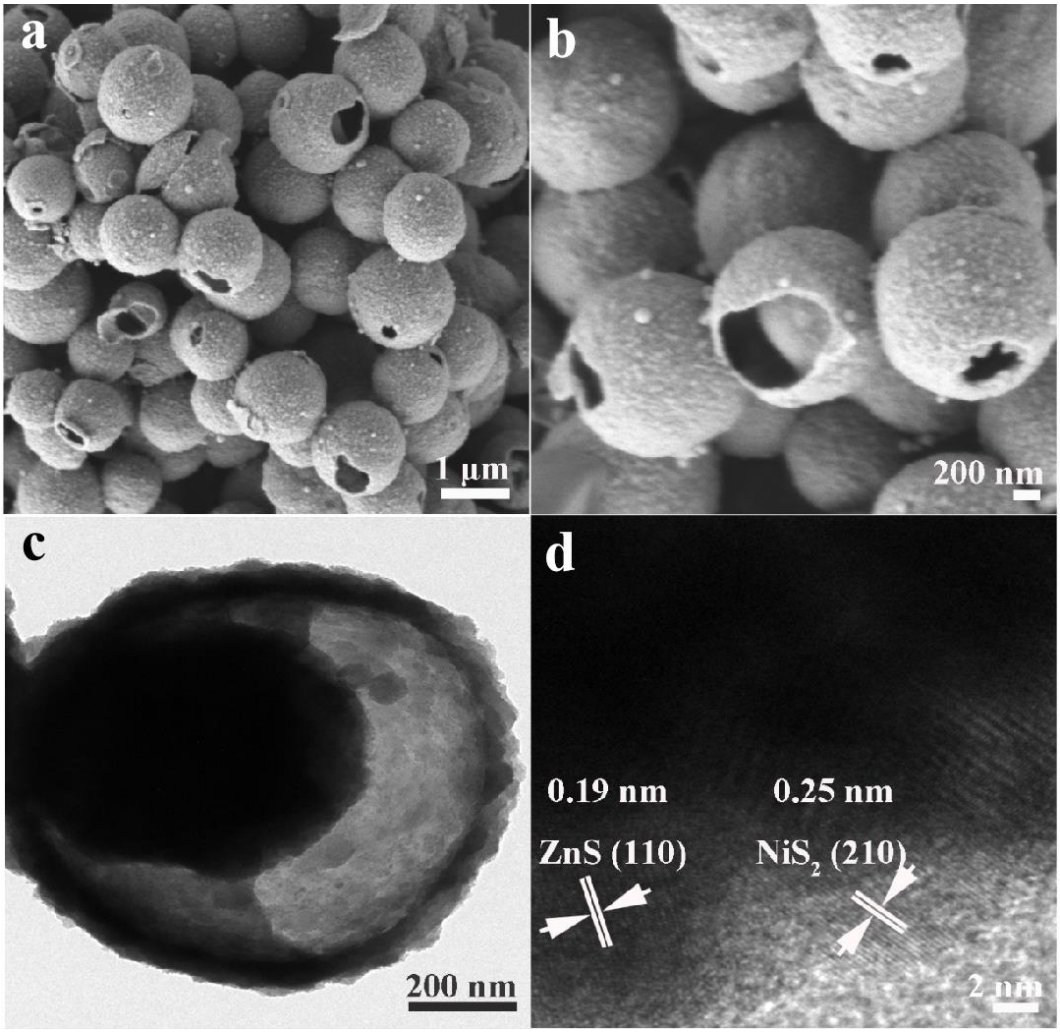

Fig. S3 FESEM (a, b), TEM (c), and HRTEM (d) images of yolk-shell NiS_2/ZnS hollow microspheres.

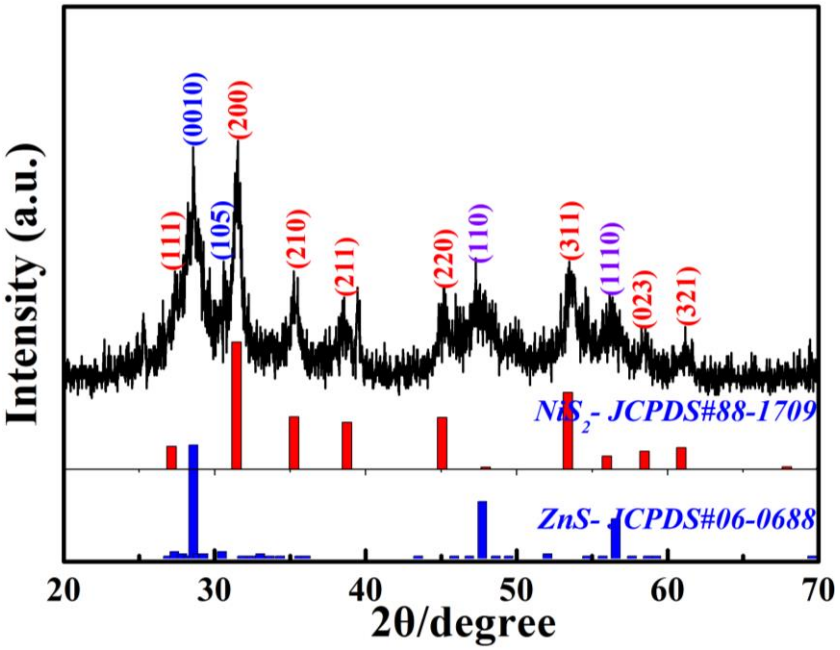

Fig. S4 XRD pattern of yolk-shell NiS_2/ZnS hollow microspheres.

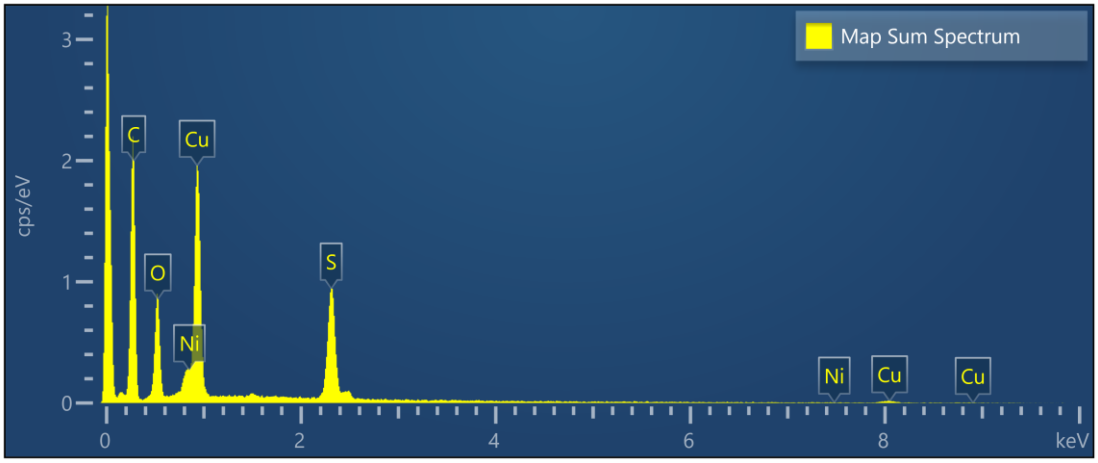

Fig. S5 EDX spectrum of yolk-shell NiS_2/CuS hollow microspheres.

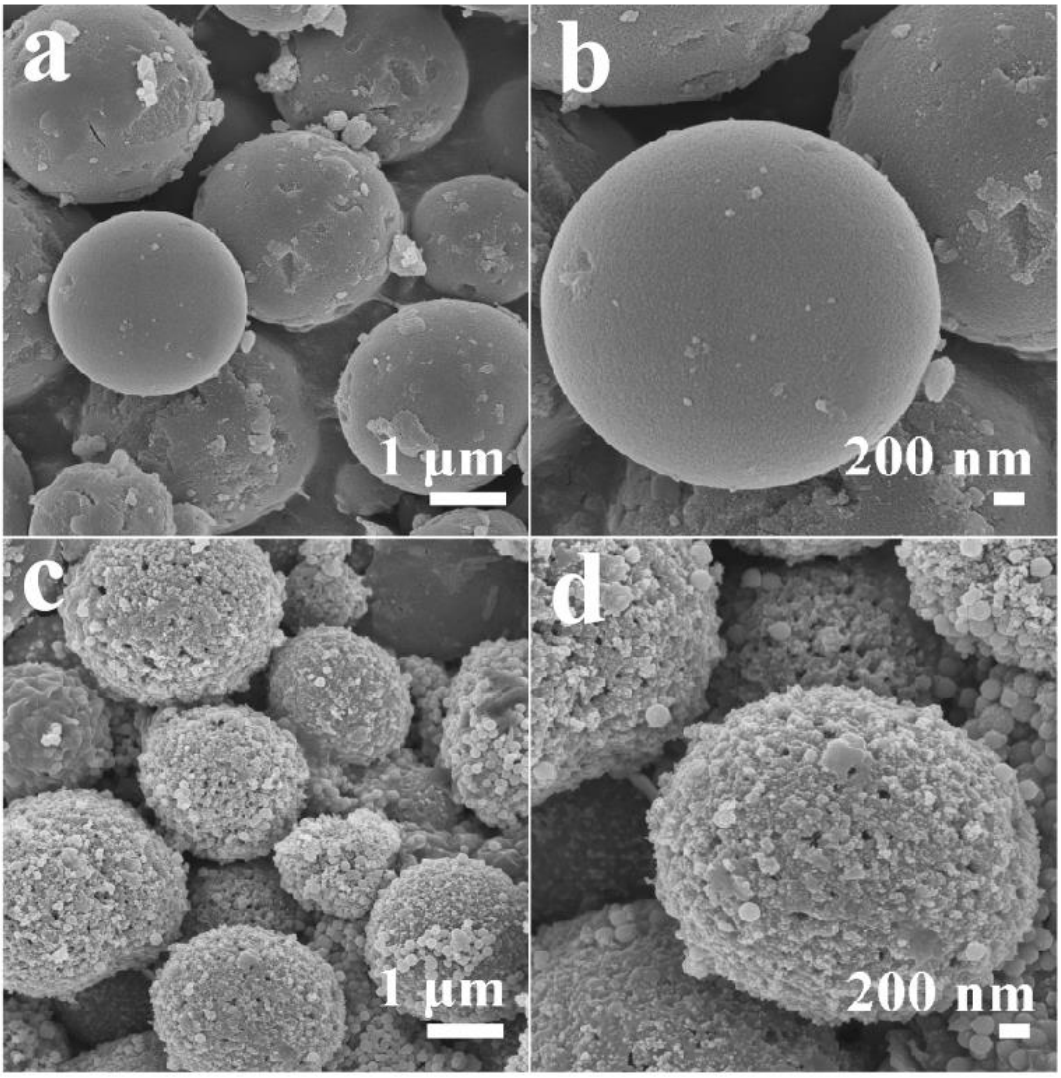

Fig. S6 SEM images of Ni-MOFs (a, b) and plain NiS_2 microspheres (c, d).

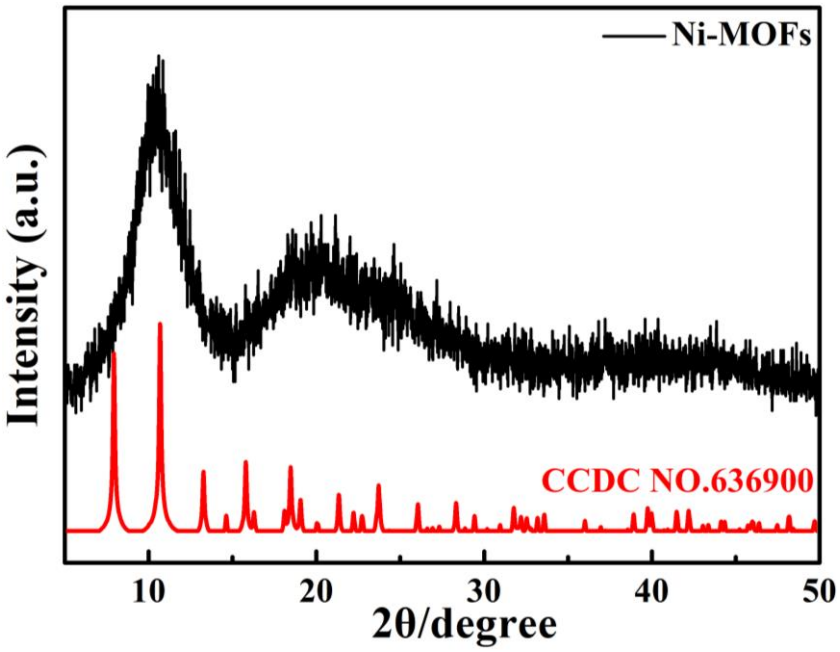

Fig. S7 XRD pattern of Ni-MOFs.

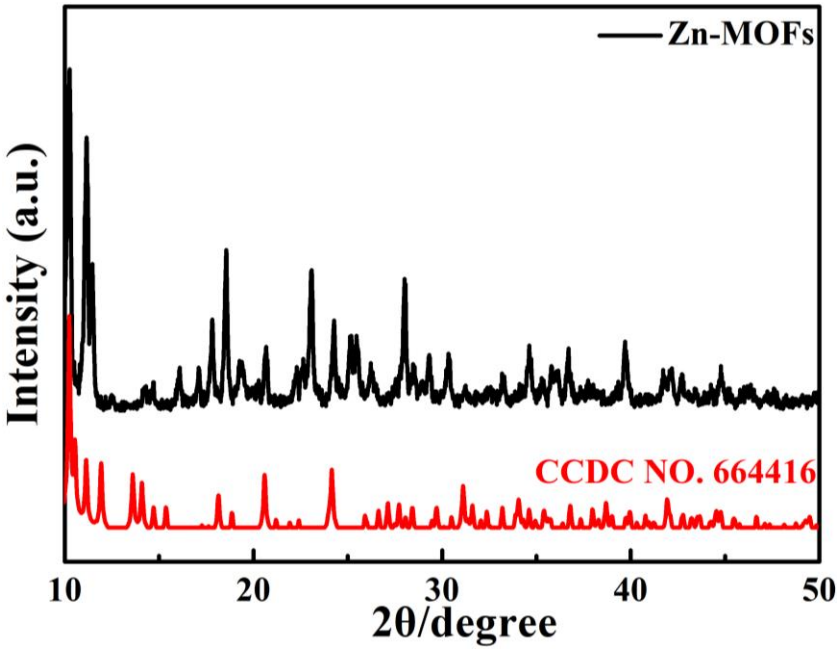

Fig. S8 XRD pattern of Zn-MOFs.

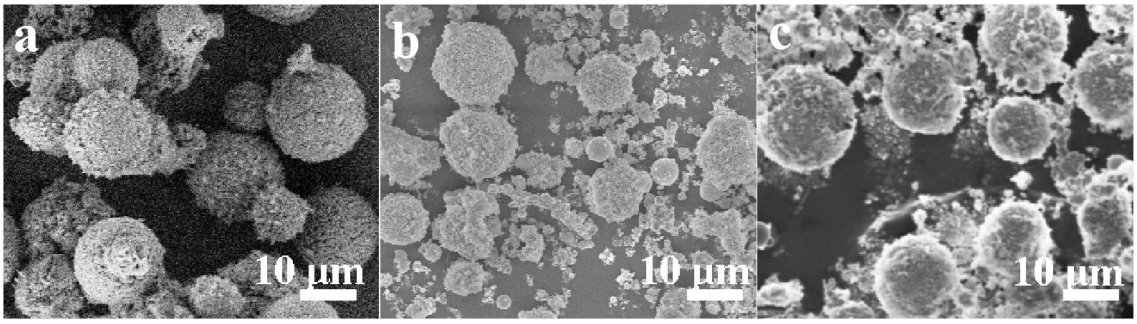

Fig. S9 SEM images of Zn-MOFs (a), ZnS (b), and CuS (c).

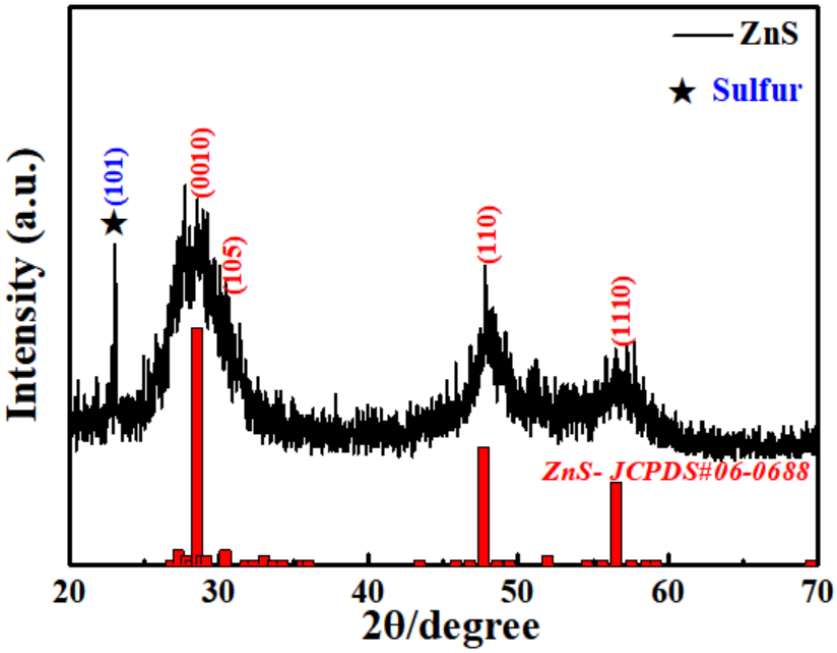

Fig. S10 XRD pattern of plain ZnS.

Table S1 ICP analysis of NiS_2/CuS and NiS_2/ZnS composites.

Samples	Cu (Wt %)	Ni (Wt %)	Zn (Wt %)	Atomic molar ratio
NiS_2/CuS	30.6	14.25	N	1 : 2
NiS_2/ZnS	N	16.48	35.98	0.49 : 1

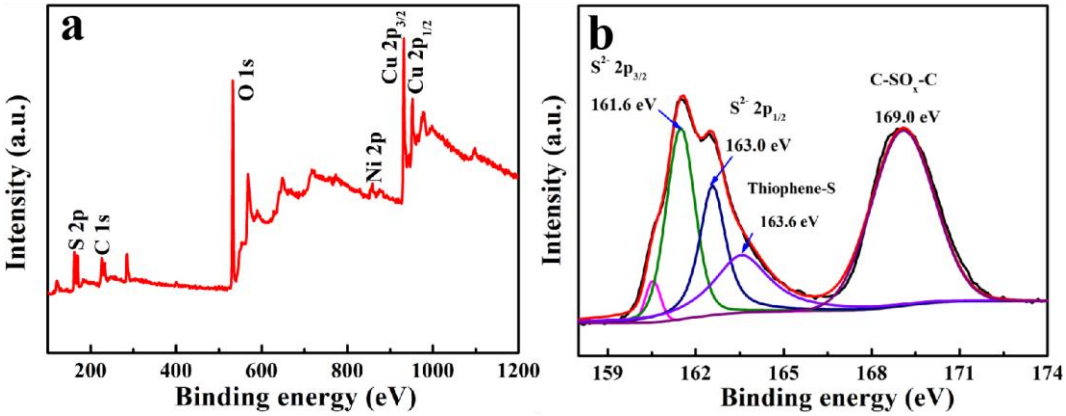

Fig. S11 XPS survey spectrum (a) and high-resolution S 2p spectrum (b) of yolk-shell NiS_2/CuS hollow microspheres.

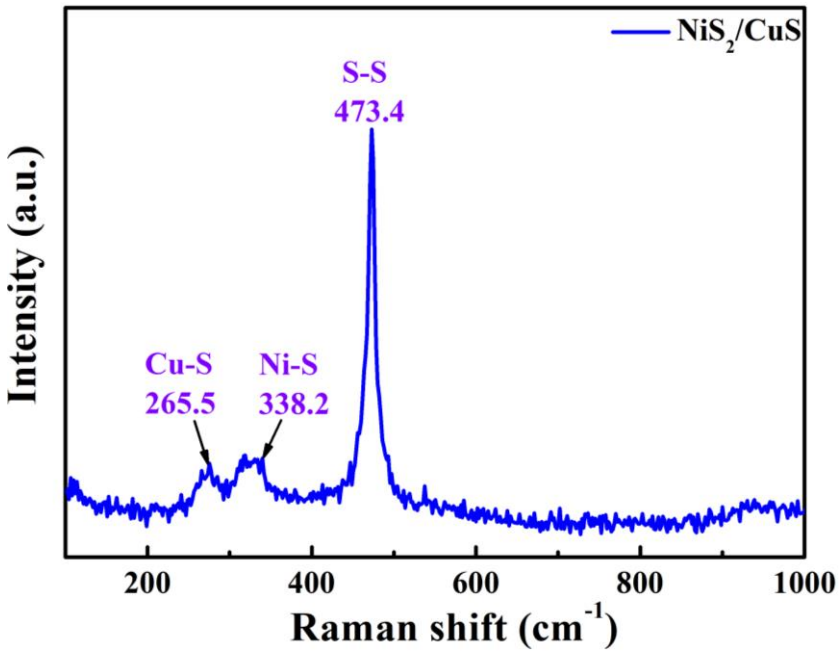

Fig. S12 Raman spectrum of yolk-shell NiS_2/CuS hollow microspheres.

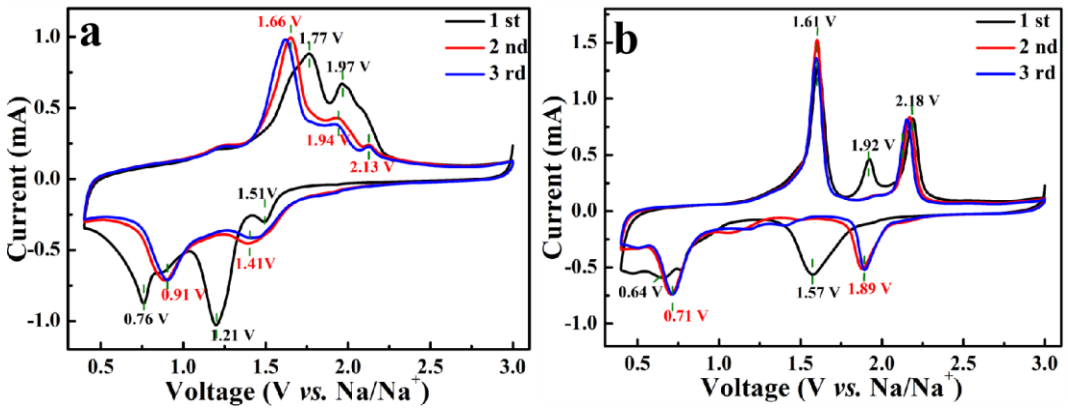

Fig. S13 The initial three CV curves of plain NiS_2 (a) and CuS (b) electrodes at a rate of 0.5 mV s^{-1} in a potential range of 0.4 ~ 3.0 V.

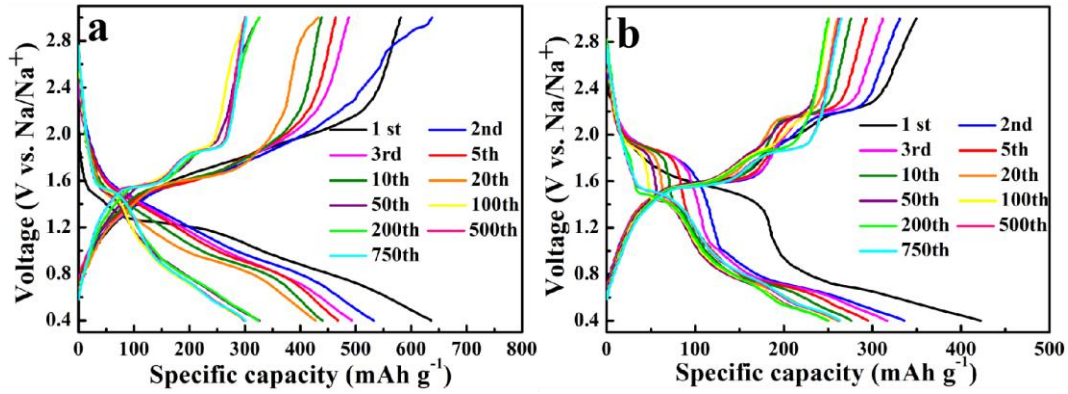

Fig. S14 The GCD profiles of plain NiS_2 (a) and CuS (b) electrodes at 2 A g^{-1} from 1st to 750th cycle in a potential range of 0.4 ~ 3.0 V.

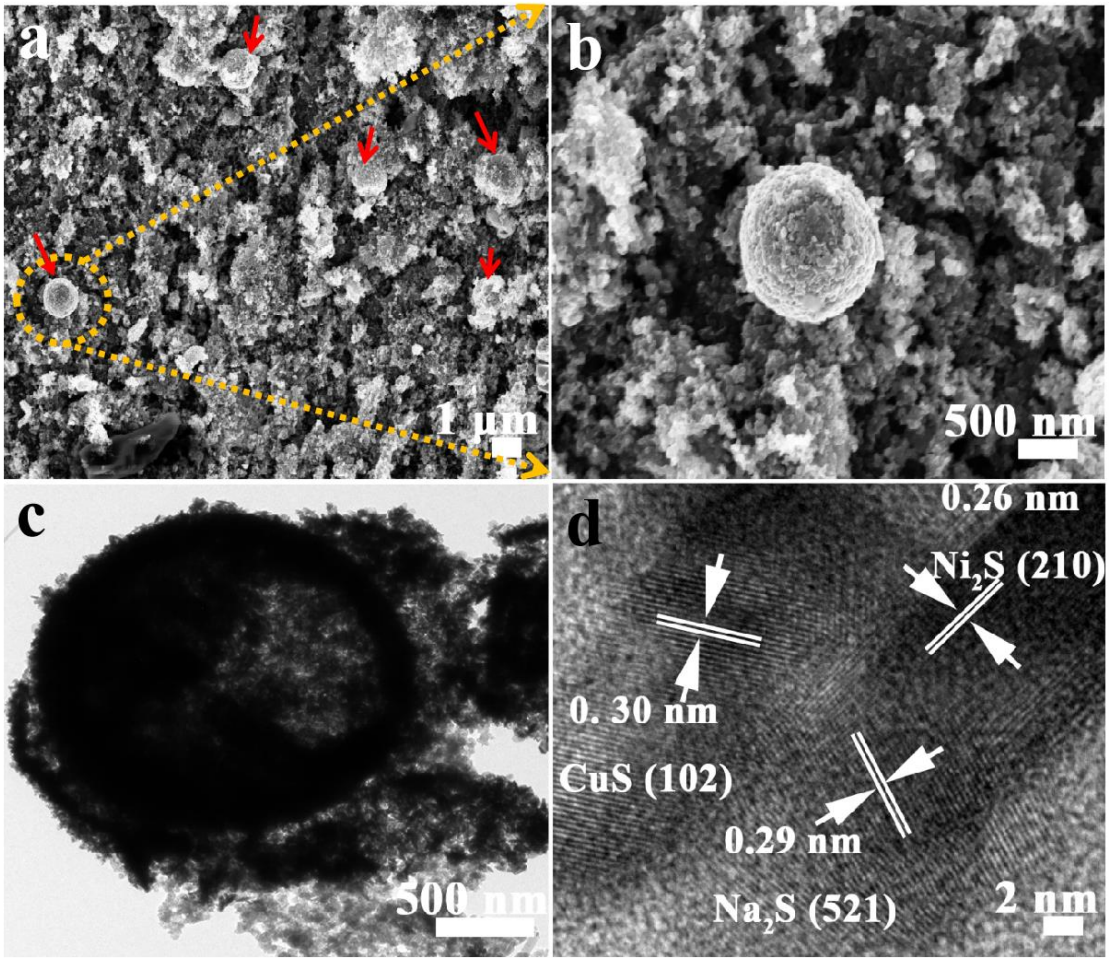

Fig. S15 The SEM (a, b), TEM (c), and HRTEM (d) images of yolk-shell NiS_2/CuS hollow microspheres after long cycles at 2.0 A g^{-1}.

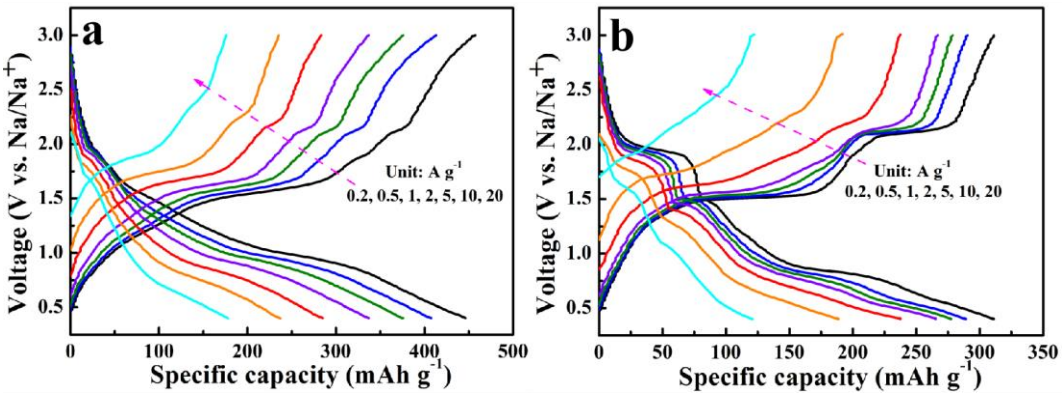

Fig. S16 The GCD profiles of plain NiS_2 (a) and CuS (b) electrodes at different current rates in a potential range of 0.4 ~ 3.0 V.

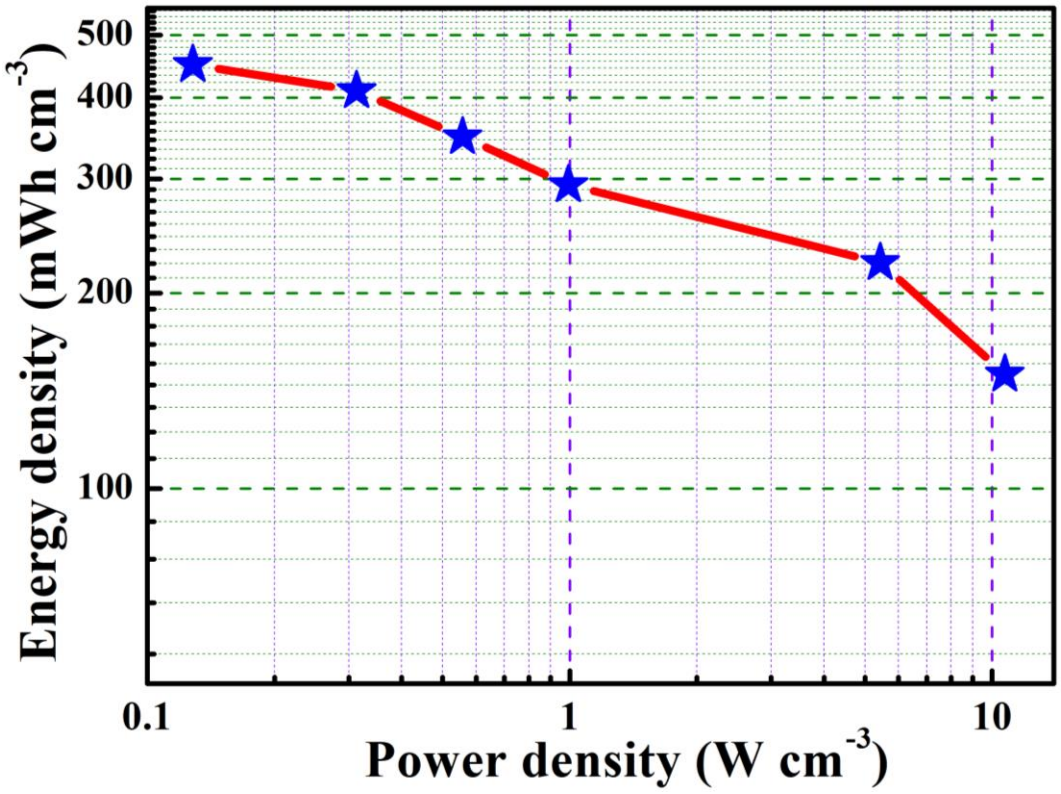

Fig. S17 Volumetric energy densities of yolk-shell NiS_2/CuS hollow microspheres at different power densities.

Table S2 A comparison of cycling performance and reversible specific capacity about NiS_2- and CuS-based anodes for SIBs.

Materials	Voltage window (V)	Rate ($A\ g^{-1}$)	Cycle number	Capacity ($mAh\ g^{-1}$)	Ref.
NiS_2@CoS_2	0.01-3.0	1.0	250	600.0	1
NiS_2 Nanospheres	0.4-2.9	0.5	1000	319.0	2
NiS_2 nanoparticles	0.01-3.0	2.0	1000	140.0	3
pomegranate-like NiS_2 nanoparticles	0.01-3.0	0.5	300	356.2	4
hollow NiS_2 spheres	0.01-3.0	1.0	300	530.0	5
SnS_2/NiS_2	0.01-3.0	2.0	100	343.2	6
NiS_2@C	0.01-3.0	0.1	100	580.8	7
CuS Microspheres	0.01-3.0	10	1000	312.5	8
CuS Microspheres	0.6-3.0	0.5	500	403.0	9
CuS@CoS_2 Double-Shelled Nanoboxes	0.4-2.6	0.5	500	403.0	10
N-Doped CuS@C Nanowires	0.4-3.0	2.0	10000	216.7	11
Platelet-like CuS	0.4-2.6	2.0	500	320	12
ZnS/CuS@C	0.4-3.0	10.0	1750	282.7	13
Hydrangea-Like CuS	0.4-2.6	1.0	400	335	14
NiS_2/CuS	**0.4-3.0**	**10.0**	**2150**	**371.6**	**This work**
		20.0	**4200**	**283.4**	

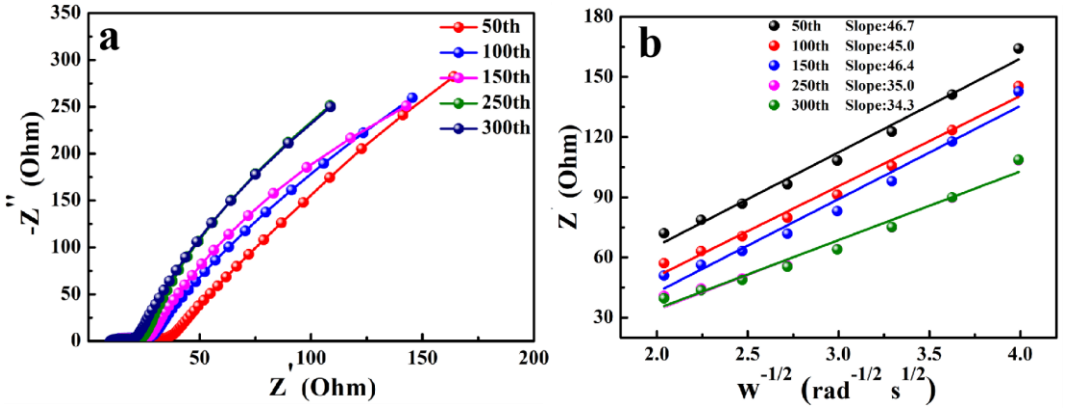

Fig. S18 Nyquist plots (a) and the linear fitting of Z and $\omega^{-1/2}$ (b) of NiS_2/CuS electrode at different cycles.

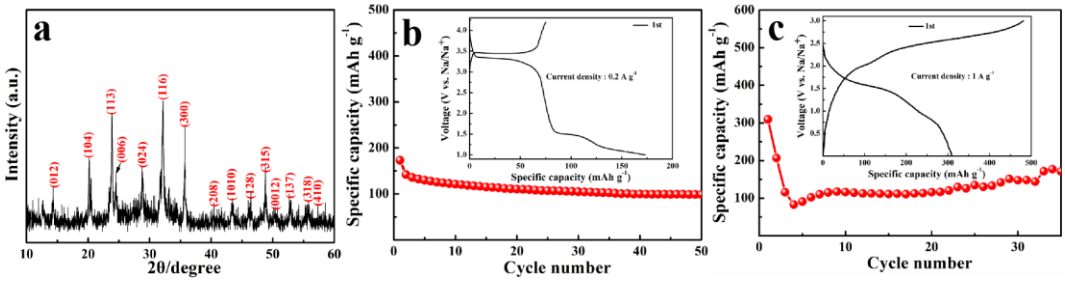

Fig. S19 (a) The XRD pattern of $Na_3V_2(PO_4)_3$@C. (b) The GCD profiles and cycling performance of $Na_3V_2(PO_4)_3$@C electrode in a potential range of 1.0 to 4.2 V at 0.2 A g^{-1}. (c) The GCD profiles and cycling performance of $Na_3V_2(PO_4)_3$@C//NiS_2/CuS full cell in a potential range of 0.01 to 3.0 V at 1.0 A g^{-1}.

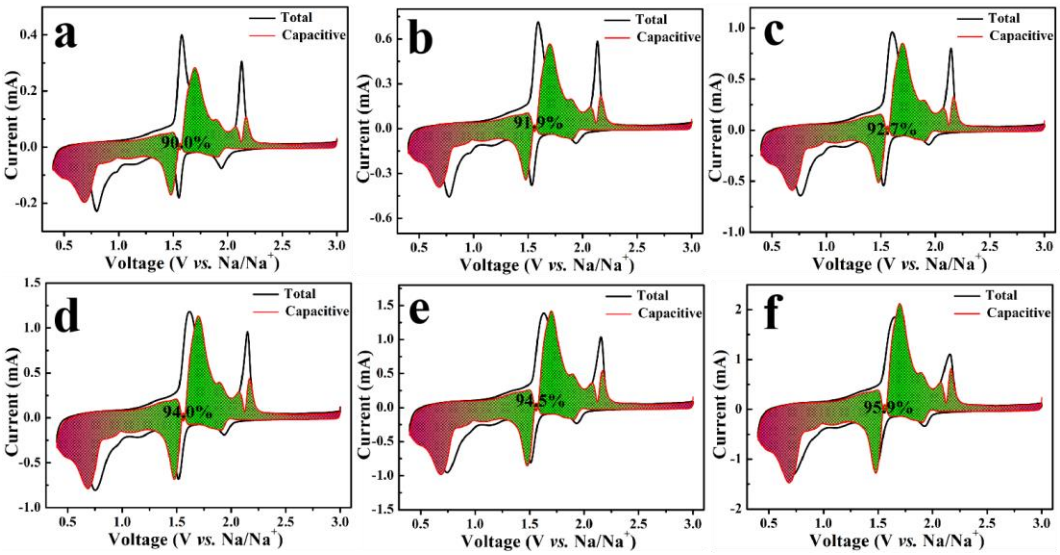

Fig. S20 The overall capacity versus pseudocapacitive fraction shown by the shaded area for NiS_2/CuS electrode at various scan rates: (a) 0.2 mV s^{-1}; (a) 0.4 mV s^{-1}; (b) 0.6 mV s^{-1}; (c) 0.8 mV s^{-1}; (d) 1.0 mV s^{-1}; (e) 1.5 mV s^{-1}.

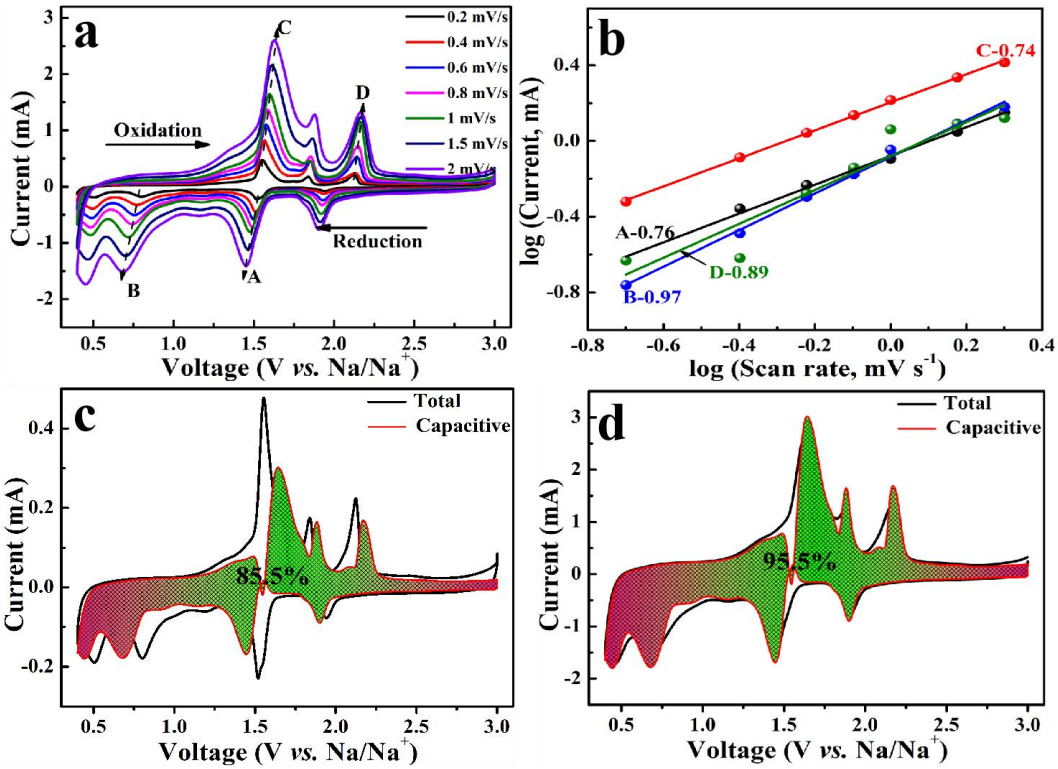

Fig. S21 (a) CV curves of plain NiS_2 electrode subjected to different scan rates from 0.2 to 2.0 mV s^{-1}. (b) The corresponding log (*i*) versus log (*v*) plots at each redox peak current. The overall capacity versus pseudocapacitive fraction shown by the shaded area at 0.2 (c) and 2.0 (d) mV s^{-1}.

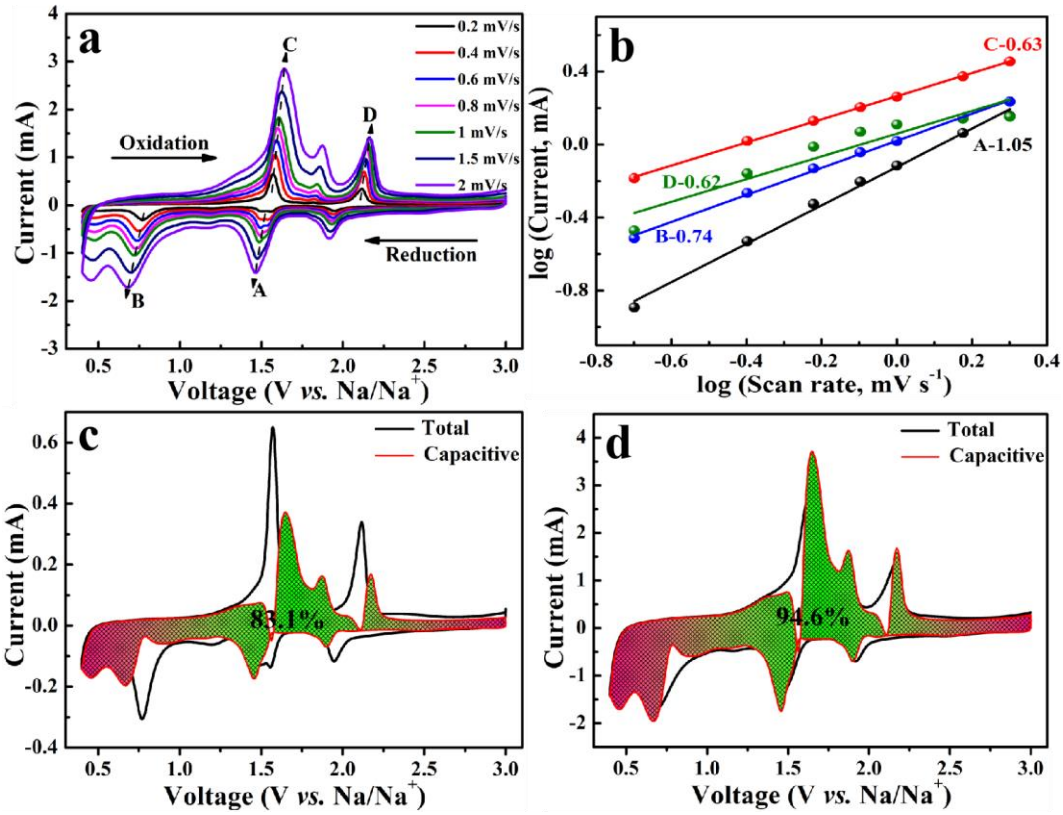

Fig. S22 (a) CV curves of plain CuS electrode subjected to different scan rates from 0.2 to 2.0 mV s^{-1}. (b) The corresponding log (*i*) versus log(*v*) plots at each redox peak current. (c) Overall capacity versus pseudocapacitive fraction shown by the shaded area at 2.0 mV s^{-1}.

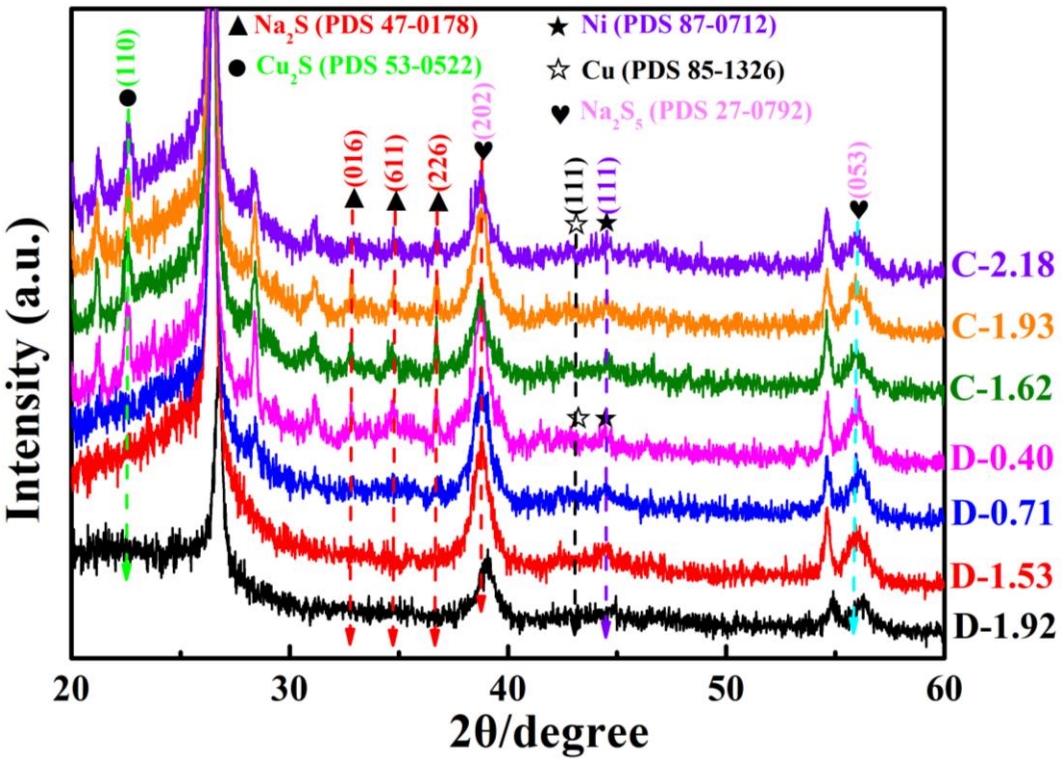

Fig. S23 The ex-situ XRD patterns of NiS_2/CuS electrode at different discharged and charged states in the second cycle.

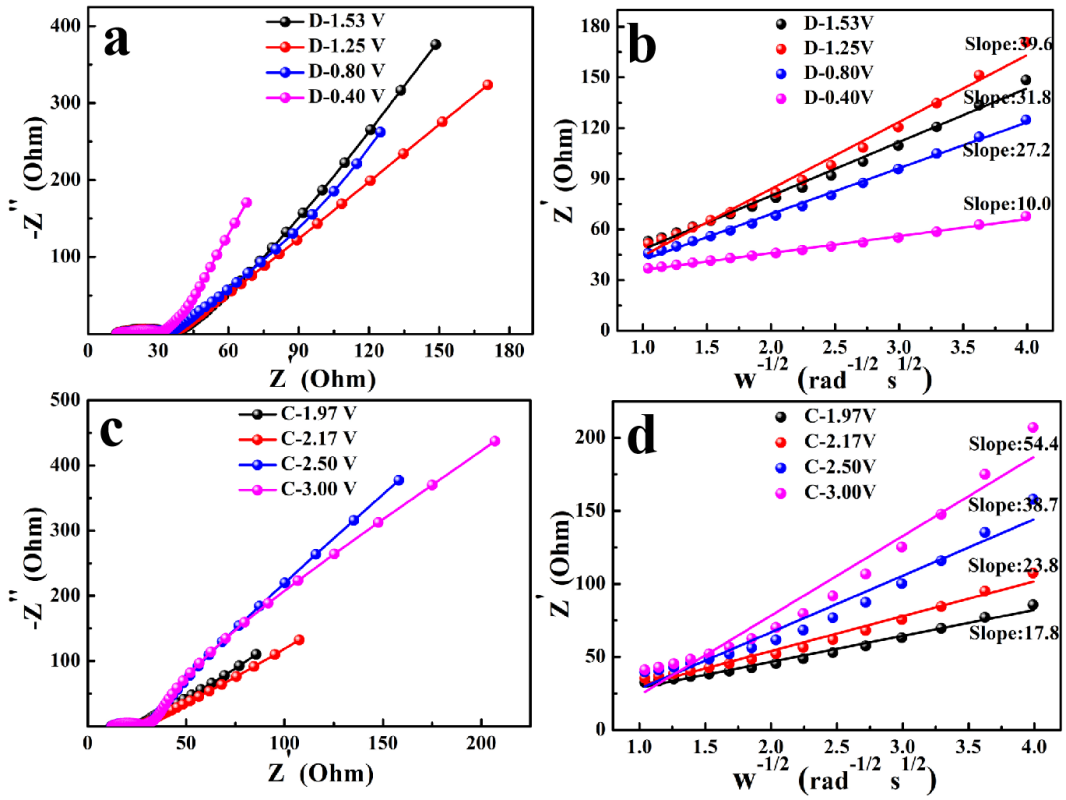

Fig. S24 Nyquist plots of NiS_2/CuS electrode at different discharged (a) and charged (c) states. The linear fitting of Z′ and $\omega^{-1/2}$ of NiS_2/CuS electrode at different discharged (b) and charged (d) states.

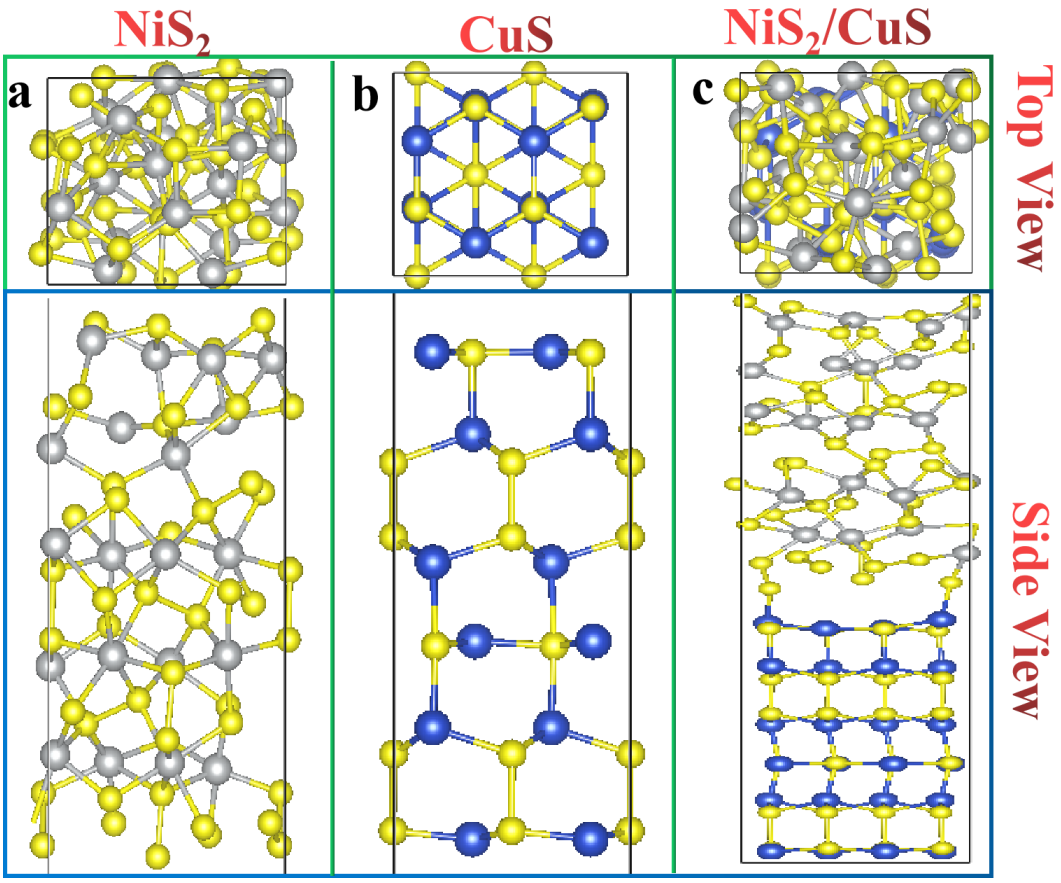

Fig. S25 Crystal structures of NiS_2 (a), CuS (b) and NiS_2/CuS (c) from top view and side view.

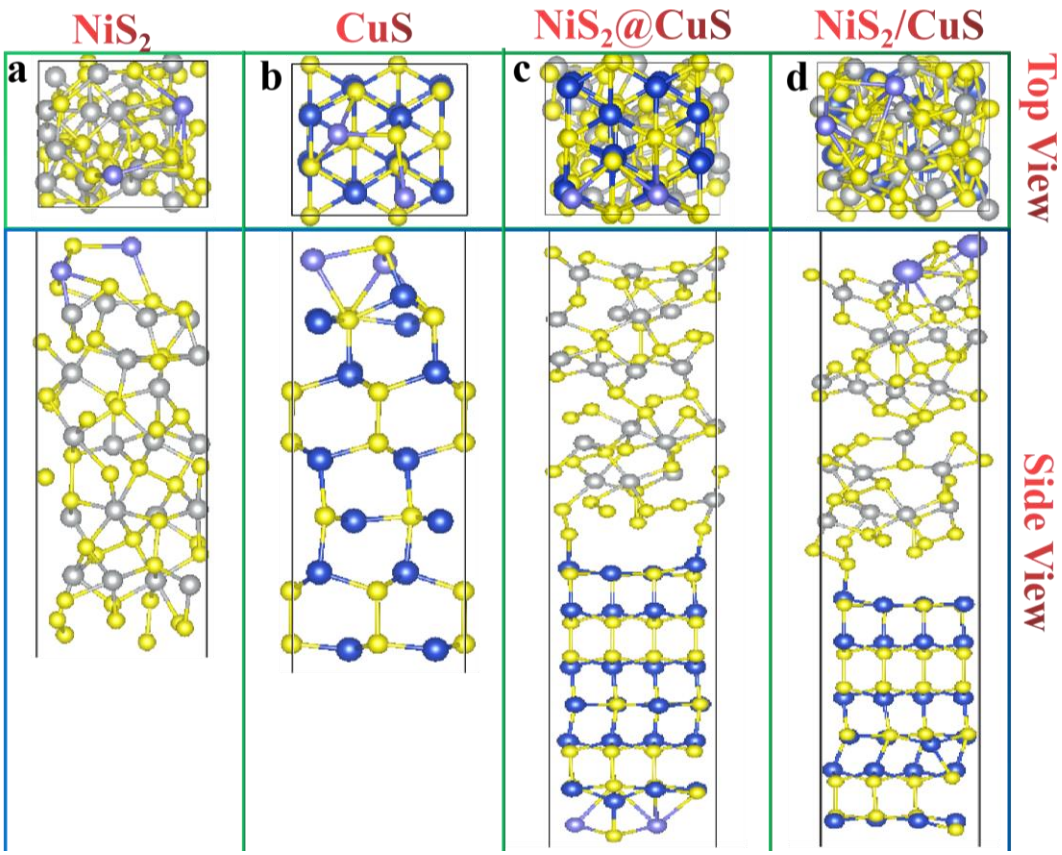

Fig. S26 The binding energies of Na_2S under the stable adsorption configuration for NiS_2 (a), CuS (b) from top view and side view. Na_2S adsorbed at CuS (c) or NiS_2 (d) crystal of NiS_2/CuS heterojunction from top view and side view.

References

1 Y. M. Lin, Z. Z. Qiu, D. Z. Li, S. Ullah, Y. Hai, H. L. Xin, W. D. Liao, B. Yang, H. S. Fan, J. Xu and C. Z. Zhu, *Energy Storage Mater.*, 2018, **11**, 67–74.

2 R. M. Sun, S. J. Liu, Q. L. Wei, J. Z. Sheng, S. H. Zhu, Q. Y. An and L. Q. Mai, *Small*, 2017, **13**, 1701744.

3 W. X. Zhao, S. Q. Ci, X. Hu, J. X. Chen and Z. H. Wen, *Nanoscale*, 2019, **11**, 4688–4695.

4 J. B. Li, J. L. Li, D. Yan, S. J. Hou, X. T. Xu, T. Lu, Y. F. Yao, W. J. Mai and L. K. Pan, *J. Mater. Chem. A*, 2018, **6**, 6595–6605.

5 R. Bi, C. Zeng, H. W. Huang, X. P. Wang and L. Zhang, *J. Mater. Chem. A*, 2018, **6**, 14077–14082.

6 S. D. Guan, T. S. Wang, X. L. Fu, L. Z. Fan and Z. J. Peng, *Appl. Surf. Sci.*, 2020, **508**, 145241.

7 G. G. Zhao, Y. Zhang, L. Yang, Y. L. Jiang, Y. Zhang, W. W. Hong, Y. Tian, H. B. Zhao, J. G. Hu, L. Zhou, H. S. Hou, X. B. Ji and L. Q. Mai, *Adv. Funct. Mater.*, 2018, **28**, 1803690.

8 Y. H. Xiao, D. C. Su, X. Z. Wang, S. D. Wu, L. M. Zhou, Y. Shi, S. M. Fang, H. M. Cheng and F. Li, *Adv. Energy Mater.*, 2018, **8**, 1800930.

9 H. Li, Y. H. Wang, J. L. Jiang, Y. Y. Zhang, Y. Y. Peng and J. B. Zhao, *Electrochim. Acta*, 2017, **247**, 851–859.

10 Y. J. Fang, B. Y. Guan, D. Y. Luan and X. W. Lou, *Angew. Chem., Int. Ed.*, 2019, **131**, 7821–7825.

11 D. Zhao, M. M. Yin, C. H. Feng, K. Zhan, Q. Z. Jiao, H. S. Li and Y. Zhao, *ACS Sustainable Chem. Eng.*, 2020, **8**, 11317–11327.

12 Z. G. Yang, Z. G. Wu, J. Liu, Y. X. Liu, S. Y. Gao, J. A. Wang, Y. Xiao, Y. J. Zhong, B. H. Zhong and X. D. Guo, *J. Mater. Chem. A*, 2020, **8**, 8049–8057.

13 W. X. Zhao, L. X. Gao, L. C. Yue, X. Y. Wang, Q. Liu, Y. L. Luo, T. S. Li, X. F. Shi, A. M. Asiri and X. P. Sun, *J. Mater. Chem. A*, 2021, **9**, 6402–6412.

14 Z. G. Yang, Z. G. Wu, W. B. Hua, Y. Xiao, G. K. Wang, Y. X. Liu, C. J. Wu, Y. C. Li, B. H. Zhong, W. Xiang, Y. J. Zhong and X. D. Guo, *Adv. Sci.*, 2020, **7**, 1903279.